A free-standing humidity sensor with high sensing reliability for environmental and wearable detection

DOI:
10.1016/j.nanoen.2022.107780

Document Version
Final published version

Nano Energy 103 (2022) 107780

Contents lists available at ScienceDirect

Nano Energy

journal homepage: www.elsevier.com/locate/nanoen

A free-standing humidity sensor with high sensing reliability for environmental and wearable detection

Yangpeiqi Yi [a], Chuang Yu [b], Heng Zhai [a], Lu Jin [a], Dongxu Cheng [c], Yifeng Lu [d], Zhongda Chen [a], Lulu Xu [a], Jiashen Li [a], Qinwen Song [e], Pengfei Yue [e], Zekun Liu [a,*], Yi Li [a,e,**]

[a] Department of Materials, University of Manchester, Oxford Road, Manchester M13 9PL, UK
[b] Department of Computer Science, University of Manchester, Oxford Road, Manchester M13 9PL, UK
[c] Department of Mechanical, Aerospace and Civil Engineering, University of Manchester, Oxford Road, Manchester M13 9PL, UK
[d] College of Architecture, Hunan University, Changsha 410082, China
[e] School of Textile Science and Engineering, Xi'an Polytechnic University, 19 Jinhua South Road, Xi'an 710048, China

ARTICLE INFO

Keywords:
Wearable humidity sensor
Free-standing structure
Sensing reliability
Washability
Carbonization

ABSTRACT

Humidity measurement has been of extreme importance in both conventional environment monitoring and emerging digital health management. State-of-the-art flexible humidity sensors with combined structures, however, lack sensing reliability when they subject to high humidity with condensation and/or liquid water invasion. Here, we report a free-standing humidity sensor by creating a stable open porous graphite structure and controlling the number of oxygen-related groups at the molecular level. The sensor indicates high sensing reliability against water liquid wetting and machine washing as well as many mechanical deformations. We demonstrate the sensor has wide potential applications in challenge environmental monitoring and wearable body area sensing networks. Particularly, the concept of the humidity sensing strategy is applicative to not only cellulose-based materials such as cotton and linen, but also protein-based materials such as silk, paving a new route for producing high-performance and cost-effective humidity sensors.

1. Introduction

Humidity detection and management play a vital role in creating a pleasant, safe, green, and energy-efficient environment. Measuring humidity within the environment has been a dramatic proliferation of research in the applications spanning from the governance of the atmosphere and soil to the management of industrial manufacture, agricultural production and physiological health [1–3]. Besides, moisture constantly evaporates from the mouth and the skin surface because of the sensible and insensible perspirations. The ubiquitous body humidity serving as a biomarker allows the construction of noncontact body area sensing networks for emerging wearable digital healthcare and well-being [4,5]. It becomes particularly important when direct-touching detection and manipulation through tactile sensors are unimplementable considering the risk of infection since the outbreak of the global Covid-19 epidemic [6]. One intriguing research prevailing in this context is to develop a flexible and high-performance humidity sensor for the abovementioned environmental and wearable detection.

Cutting-edge flexible humidity sensors are always fabricated by combining humidity-response materials with soft substrates through physically coating or blending [6–10]. However, the active materials in the combined configuration are neither wettable nor machine washable due to the loss and/or redispersion of the active materials when interacting with water. It greatly limits practical applications as humidity sensing frequently subjects to high humidity condensation and interaction with liquid water. On the other hand, such laminated structure sensor fails to avoid interference from mechanical deformations, which deteriorates the sensing reliability and accuracy in practical humidity monitoring. It has been a critical challenge to explore a straightforward approach to develop a free-standing humidity sensor with outstanding wettability, washability, and sensing reliability when exposing to challenging environments.

Herein, this work proposes a humidity sensing strategy by creating a stable open porous graphite structure and controlling the content of functional groups based on waste textiles. The humidity sensor shows tunable initial resistance and sensitivity by controlling carbonization

* Corresponding author.
** Corresponding author at: Department of Materials, University of Manchester, Oxford Road, Manchester M13 9PL, UK.
E-mail addresses: zekun.liu@manchester.ac.uk (Z. Liu), henry.yili@manchester.ac.uk (Y. Li).

https://doi.org/10.1016/j.nanoen.2022.107780
Received 17 June 2022; Received in revised form 11 August 2022; Accepted 6 September 2022
Available online 9 September 2022

temperature and oxidation degree respectively. Due to the free-standing configuration (the humidity-response material is the substrate itself), the sensor exhibits prominent reliability to water liquid wetting and machine washing, and negligible dependence to mechanical inputs and geometry deformation. We innovatively explore the humidity sensing mechanism by correlating absorbed humidity weight and electrical response to reflect electrical response capacity to unit moisture content. The sensor is successfully demonstrated for the detection of atmospheric humidity and soil wetness, hand gesture and motion, as well as various respiration models. Noteworthy to mention that it first finds carbonized fabric (CF) can detect humidity and the oxidated carbonized fabric (OCF) sensor with an improved sensitivity by further oxidation. Importantly, we prove that this strategy is applicative to many substrates (e.g., cotton, linen, and silk) as a new strategy for flexible, eco-friendly, and high-performance humidity sensors.

2. Experimental section

2.1. Fabrication of the CF and OCF sensors

Waste cotton woven fabrics (supplied by the textile lab, University of Manchester) were carbonized in a tube furnace with nitrogen atmosphere with heating rate of 2 °C/min. After reaching carbonization temperature, samples naturally cooled down to room temperature. The oxidation was performed by immersing the CFs in a sulfuric acid/nitric acid mixture (v/v 3:1) at 70 °C for 1, 2, 3 h respectively to induce the growth of functional groups. The sulfuric acid (>=95%, Analytical reagent grade) was purchased from Fisher Chemical. The nitric acid (70%, Analytical reagent grade) was purchased from Sigma Aldrich. After oxidation, samples were washed in distilled water three times and dried overnight in fume cupboard. The CF and OCF samples were finally cut into the size of 3 × 2 cm^2 with conductive tapes at both ends for the fabrication of humidity sensors.

2.2. Material and sensor characterizations

The surface morphology and structure of the CFs and OCFs were characterized by a SEM (ZEISS Ultra-55) and TEM (Tecnai T20). The atomic percentage and element distribution were detected by the SEM (Quanta 200) equipped with energy-dispersive X-ray spectroscopy (EDS). We evaluated mechanical performance of samples by a universal mechanical testing machine (Instron 3344 L). Raman spectra were performance with a Raman spectroscopy (WITec, Apyron) with a laser excitation wavelength of 532 nm. X-ray Photoelectron Spectroscopy (XPS) analysis was performed using an Axis Ultra Hybrid spectrometer (Kratos Analytical, Manchester, United Kingdom). Water drops (2 μl) in wettability test were applied by Kruss Drop Shape Analyzer (DSA100) to observe the dynamic contact angle change. The sheet resistance of the CFs and OCFs (N = 3) was measured following four-point mode of Keithley 2450 at 25 °C and 50% RH. Humidity sensing performance of sensors was implemented in a conditioning cabinet (Datacolor CONDITIONE), the RH is programmable from 30% to 90%. To achieve the higher humidity level (i.e., > 90% RH), 100 mL boiled water was placed inside the cabinet. A commercial humidity sensor (Sensirion SHT4x Smart Gadget) monitored the humidity during experiments. We collected the electrical signals of sensors through Keithley 2000/2450. The evaporation rate of the sensors was characterized via dropping water (~40 μl) on samples in a room with fixed temperature and humidity, where a multimeter and a thermal camera (FLIR-C3) and were used to measure resistance and temperature change of sensor surface respectively. We measured electrical signals, weight absorption, and humidity level of sensors (N = 3) to investigate their relationship by synchronously using a multimeter, a precise balance (Mettler, AE100) from 40% to 90% RH in the humidity cabinet (21 ℃). Washability was evaluated by washing the OCF-3 h sensor at room temperature through a commercial washing fastness tester in pure water according to BS EN ISO 105 C06A1S. Air permeability was measured by the instruments of SDL ATLAS AirPerm.

2.3. Application demonstrations

Atmospheric humidity monitor was implemented by attaching the OCF-3 h sample onto a drone (DJI FPV) with a wireless data transmission setup (i.e., NFC antenna and smartphone) [11]. We flew the drone to 30 m and 200 m height with a 5 min hover, respectively. The initial humidity level was recorded based on the commercial sensor and the humidity in 30 m and 200 m was calculated through the sensor characterization. Environmental/soil humidity monitoring system was achieved by embedding the sensor inside the soil (1 cm depth) and attaching another one above the soil (1 cm height). Before the experiment, soil was dried at 80 °C overnight. The water drainage in soil was demonstrated through embedding three sensors at 1 cm, 2 cm, and 3 cm under the soil. Multi-channel wireless data transmission system including Bluetooth-based signal processing unit (TruEbox), and visualization software (TruEbox-01RC) matched with smartphone was supplied from LinkZill Technology Co., Ltd (Hangzhou, China).

3. Results and discussion

3.1. Molecular engineering humidity sensor demonstration

Fig. 1a illustrates the fabrication of the OCF humidity sensor via step-by-step functionalization through two steps: carbonize pristine cotton fabric under 600 °C to induce the transformation from cellulose to pseudo-graphite structure; immerse the CF in an acid mixture to promote the in-situ growth of oxygen-related groups on fiber surfaces (see details in Experimental Section). The OCF enables to capture and absorb the moisture from surroundings due to the functional groups. Proton hopping within the bonded consecutive water molecules decreases the OCF resistance, implementing humidity sensing by converting humidness into electrical outputs. (Fig. 1b) [7,12]. The free-standing OCF sensor is capable of monitoring environment by detecting atmospheric humidity, plant moisturizing, and the soil water content in extreme conditions (Fig. 1c). It also shows potential in emerging wearables for digital wellbeing, respiration monitoring, and noncontact interfaces by constructing body area humidity sensing networks (Fig. 1d).

3.2. Materials characterization

The functionalization significantly changes the molecule structure. With thermal degradation, the fabric undergoes both surface shrinkage and weight loss, while it remains fabric structure (Fig. S1a-c). Neither the carbonization nor oxidation destroys the fiber integrality, they evenly motivate the element transformation of fiber surfaces (Figs. 2a, b and S1d, e). The carbonization-induced structure transformation from cellulose to pseudo graphite is confirmed by observing many tiny distorted lattice stripes with an interlayer distance of ~0.35 nm in a typical transmission electron microscope (TEM) image (Fig. S2a), of which observation is consistent with previous work [13,14]. The strain-stress curves of the CF, OCFs (Fig. 2c), and pristine cotton fabric (Fig. S2b) show that both carbonization and oxidation deteriorate their breaking strain and stress, while the OCF-3 h remains high breaking stress of ~0.24 MPa. Figs. 2d and S3a displays that the conductivity of the CF is significantly affected by carbonization temperature, where sheet resistance drops from 1.56 × 10^6 to 5 Ω/sq when temperature from 600 °C to 1000 °C. The improvement in conductivity is attributed to the temperature-induced increase in structural order, which is proved by the full width at half maximum (FWHM) in the Raman D-band (Fig. S3b-f) [15]. On the other hand, enhanced oxidation time gradually weakens the conductivity, which is due to the increase of defects in the pseudo-graphite structure (Fig. 2e). We evaluate the defects by comparing the I_D/I_G ratio, of which ratio is 0.89 and 1.11 for the CF and

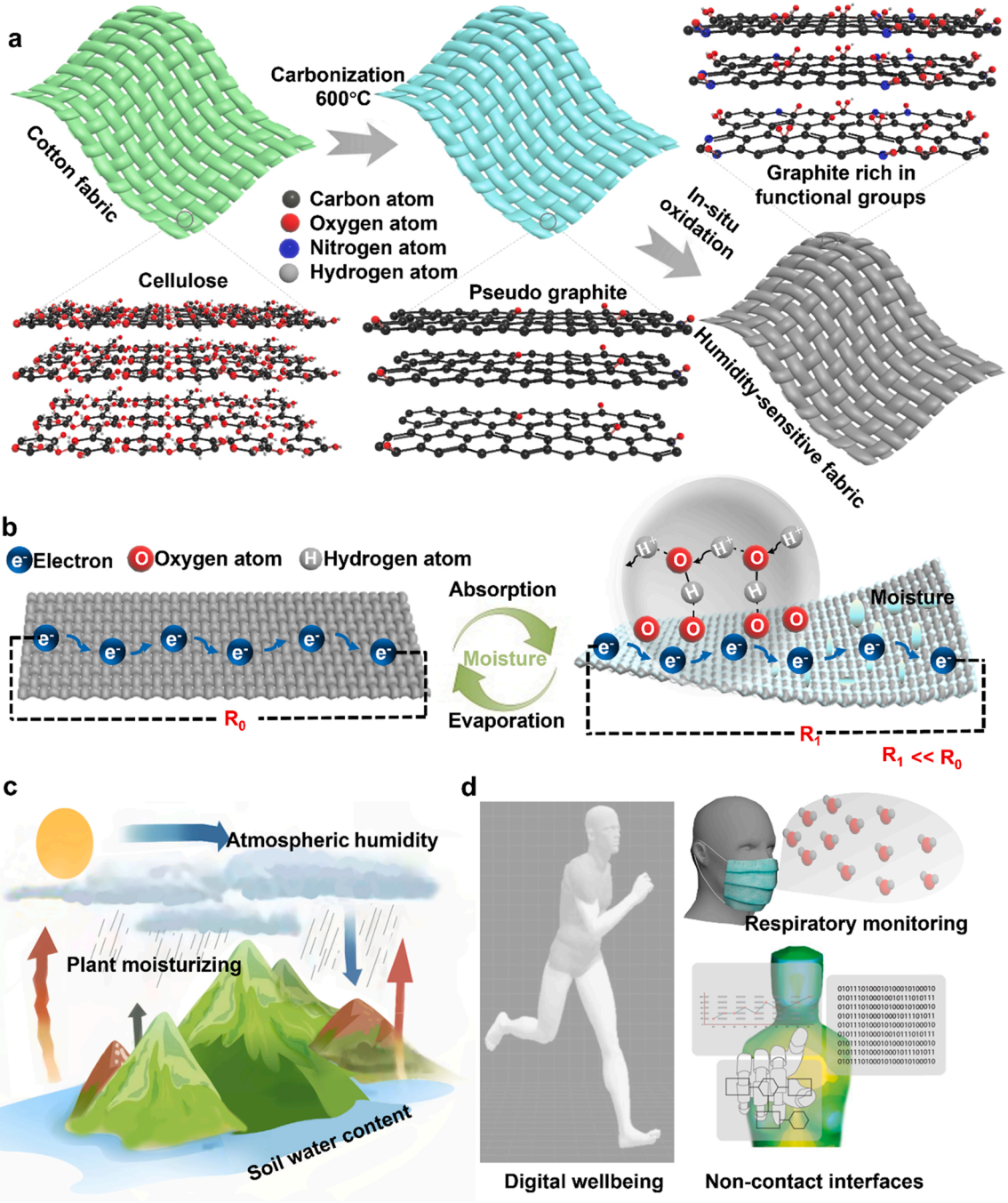

Fig. 1. Illustration of fabrication and applications of the OCF humidity sensor. (a) Step-by-step structural transformation of the cotton fabric after carbonization and oxidation. (b) Working mechanism of the OCF sensor, where proton hopping increasing the amount of moving electrons and decreasing the resistance. Proof-of-concept demonstration of the OCF sensor in (c) environmental and (d) wearable detection.

OCF-3 h respectively (Fig. S4). Such trend is in agreement with reported work [16,17].

Surface elements and hydrophilicity also change as a function of carbonization and oxidation. The wide-scan X-ray spectroscopy mapping (XPS) spectrum (Fig. 2 f), high-resolution spectrum of the C 1 s peak (Fig. 2 g), and high-resolution spectrum of the N 1 s peak of the fabrics show that their chemical state of the heteroatoms with increased oxidation time. By fitting the C 1 s peak at the binding energy of 284.1 eV (belonging to C═C), 284.8 eV (belonging to C-C), 285.5 eV (belonging to C-O), 286.8 eV (belonging to C-O-C), 288.4 (belonging to O-C═O), and 290 (belonging to π-π *) [15,16,18,19]. It indicates that the O content rises from 17.7% to 30.9%, while the C drops from 80.2% to 66.3% after oxidizing for 3 h (Fig. S5a). The C═O and O-C═O percentages sharply raise after oxidating treatment, and then slightly increase with the enhancement of oxidation time (Fig. S5b). A new nitrogen oxide species peak at ~405.7 eV (Figs. 2h, and S5c) confirms the existence of -NO_x [13,20,21]. The functional groups on the OCFs have significant improvement in surface hydrophilicity. Fig. 2i shows the CF acquires a contact angle of 111.7° (at 0 s), and the contact angle gradually drops with time. The instantaneous contact angles throughout 0–30 s decrease with the increase of oxidating time (Fig. S6). The contact angle of the OCF-3 h at 0 s is just 13.7° (Fig. 2j), and it can absorb most of the water droplet within a short period (~5 s). On the contrary, incremental carbonization temperature deteriorates surface

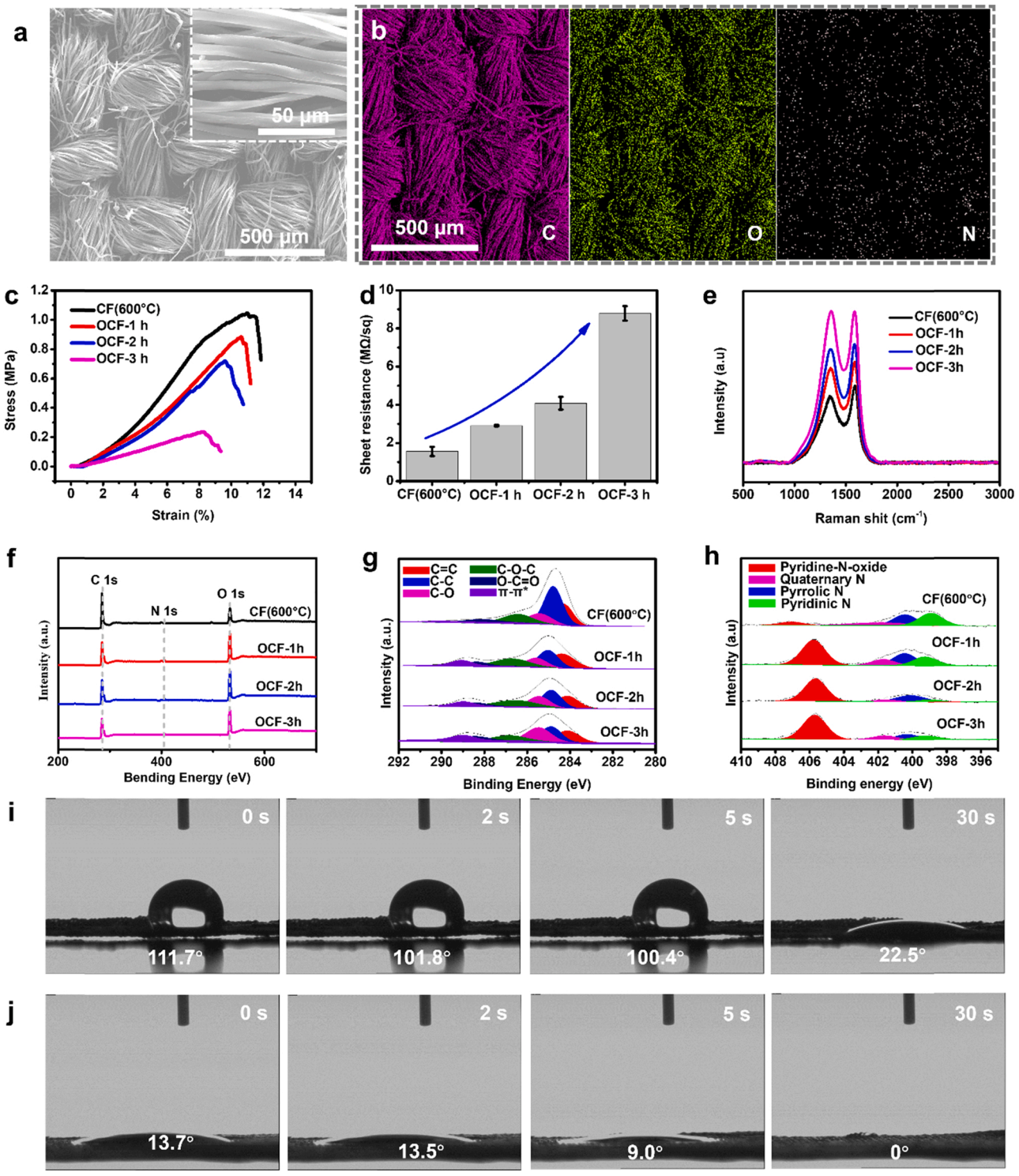

Fig. 2. Characterization of the CF and OCFs. (a) Surface morphology (the insert is high magnification SEM of fibers), and (b) surface element distribution of the OCF-3 h. (c) Strain–stress curves, (d) sheet resistance, (e) and Raman spectra of the CF, OCF-1 h, OCF-2 h, and OCF-3 h. (f) Wide-scan XPS spectrum, (g) high-resolution XPS spectrum of the C1s XPS peak, (h) and high-resolution XPS spectrum of the N 1 s XPS peak for the CF, OCF-1 h, OCF-2 h, and OCF-3 h. Photographs of water droplets on (i) the CF, and (j) the OCF-3 h, showing their surface hydrophilicity.

hydrophilicity. Both the CFs (800 °C, and 1000 °C) have a higher contact angle at corresponding time (Fig. S7), and the water droplets are not completely absorbed after 30 s

3.3. Humidity response and sensing mechanism

We explore the carbonization temperature and oxidation time in determining the electrical response to humidity. Fig. 3a shows the electrical change of the CF (600 °C) is less than that of the OCF sensors when directly moving them into a chamber with relative humidity (RH) of 90% from room ambient (~50% RH). The response rises as a functions of increasing oxidation time, which is highly stable and reproducible from patch to patch (Fig. 3b). It also shows enhanced oxidation endows the sensor with a slower recover speed. This is because oxidation

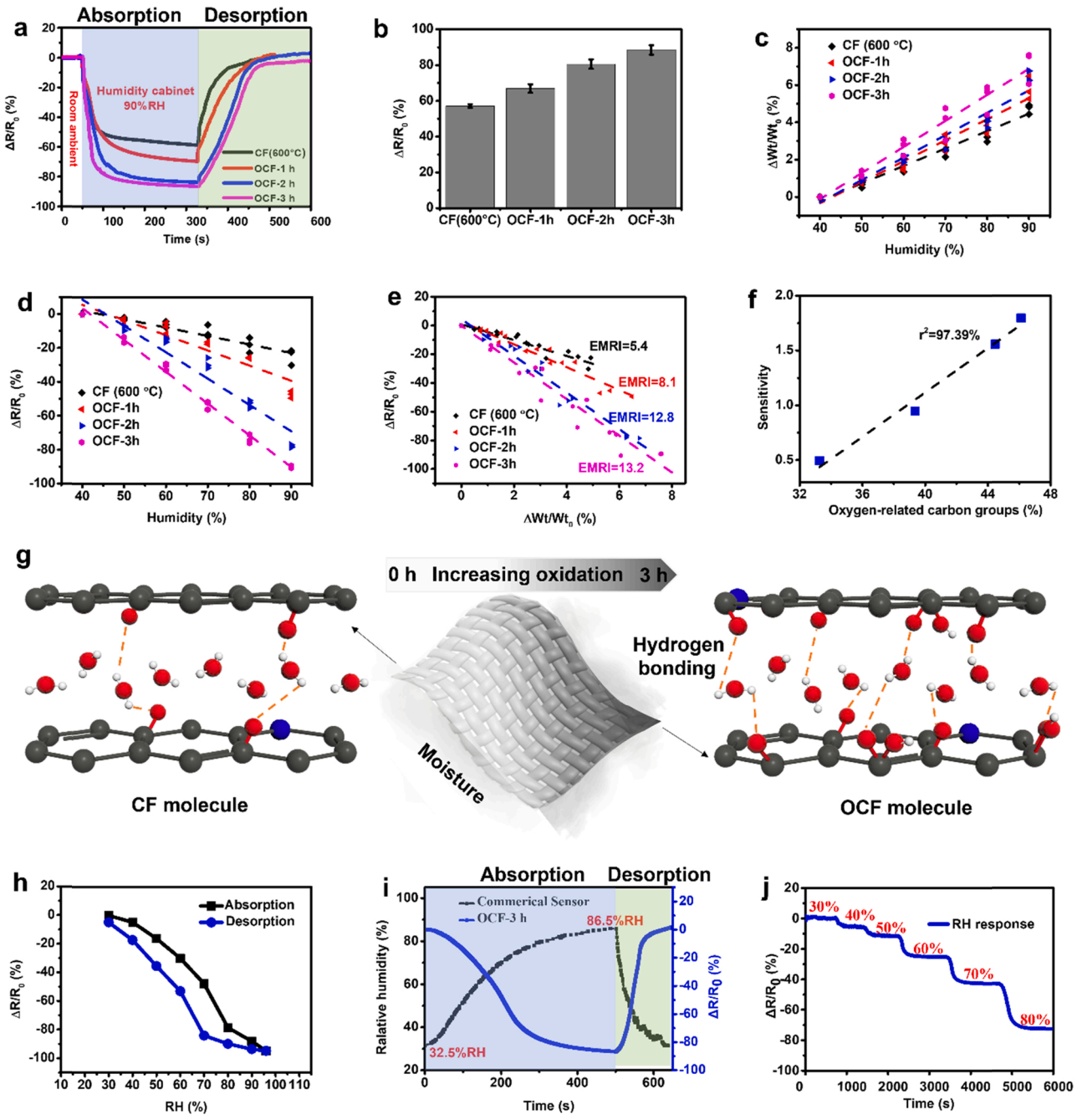

Fig. 3. Electrical response of the CF and OCF sensors, and the sensing mechanism. (a) The relative resistance changes of the sensors by moving them inside a chamber with 90% RH from room condition (~50% RH). (b) The maximum electrical change of the sensors from patch to patch, showing the functionalization is stable and reproducible. (c) Moisture sorption isotherm. (d) Electricity -humidity response isotherm. (e) Electricity-moisture sorption isotherm. The EMRI refers to electricity-moisture response index, showing sensors' electrical response to per unit moisture. (f) The relationship between sensors' sensitivity and their OCGs. (g) Humidity sensing mechanism illustration. (h) Electrical signals of the OCF-3 h sensor in absorption-desorption humidity. (i) Comparison between the OCF-3 h sensor and a commercial humidity sensor in absorption-desorption RH from 32.5% to 86.5%. (j) Dynamic electrical response of the OCF-3 h sensor to step-by-step increasing RH from 30% to 80%.

increased groups bond with large content of water molecules in the molecular chain, it takes more time to get released. This phenomenon is additionally confirmed by wetting the sensor with the same amount of water liquids and observing the electrical recover. It indicates moisture evaporation by absorbing heat (insert images) takes more time when the sample with raised oxidation time (Fig. S8). The electrical change of the CF sensors carbonized in 800 °C and 1000 °C is very limited (Fig. S9a). It can be explained by the lower amount of oxygen element on the CF surface after higher temperature carbonization (Fig. S9b). Noted that the CF carbonized in 400 °C owns too high electrical resistance to measure, which is not suitable to detect humidity. Besides, we oxidized the CF carbonized in 800 °C. The electrical response towards humidity enlarges with increased oxidation time (Fig. S10). It exhibits the validity of oxidation treatment in enhancing the electrical change no matter what the carbonization temperature is. Through controlling carbonization temperature and oxidation time, the sensors reveal tunable initial resistance and sensitivity (Table S1), which is of prime importance to adapt practical applications. we treated other textiles to further verify

the effectiveness and expansibility of the functionalization strategy. It proves this approach is extendable to linen (Fig. S11a-c) and silk fabrics (Fig. S11d-f), which means that the carbonized linen and silk fabrics are capable to detect humidity, and more importantly, their sensitivity can be further improve by oxidation as well.

We investigate the sensing mechanism by correlating functional group content of the CF and OCF sensors (600 °C) with their electrical response at different humidity level in absorbing humidity process (detailed setup in Experimental Section). Moisture sorption isotherm (Fig. 3c) and electricity-humidity response isotherm (Fig. 3d) show that the sensors experience resistance decrease with absorbing moisture. Oxidation treatment improves both moisture sorption capacity and electrical response ability. The relationship of absorbed water, RH, and oxygen-related carbon group (OCG) is given by Eq. (1), the relationship of absorbed water, electrical change, and OCG is given by Eq. (2).

$$WWC = 0.001166\ RH + 0.000827\ OCG - 0.08278 \quad (1)$$

$$RC = -10{\cdot}513\ WWC - 0.01537\ OCG + 0.6544 \quad (2)$$

By integrating Eq. (1) into Eq. (2), we can get Eq. (3).

$$RC = -0.01226\ RH - 0.02406\ OCG + 1{\cdot}5274 \quad (3)$$

According to the Eq. (3), RH is given by.

$$RH = -81{\cdot}5\ RC - 1{\cdot}962\ OCG + 205{\cdot}87 \quad (4)$$

Where the WWC, RH, RC, and OCG refer to relative water weight change (%), environmental relative humidity RH (%), relative resistance change (%), and OCG content (%) respectively. Based on Eq. (4), RH can be correlated to the RC and OCG of sensors. We expect it can calculate humidity level by directly measuring the OCG content and RC. According to the relationship between the WWC and RC (Fig. 3e), we define an index: electricity-moisture response index (EMRI) (i.e., absolute value of slope) to reflect electrical response capacity to unit moisture content. The humidity sensor acquiring a larger EMRI shows a higher sensitivity. Our theoretical hypothesis is that the OCG on the graphite sheets can attract moisture molecules and polarize them. The absorbed moisture molecules can bridge the graphite sheets by linking with the OCG on different sheets. The more OCG forms more bridges, thus leading to a higher sensitivity. By comparing the sensors' sensitivity with their OCG content, it reveals the sensitivity is positively related to the amount of the OCG (Fig. 3f), which supports our hypothesis. The proposed humidity sensing mechanism in molecular level in Fig. 3g shows oxidation-induced enhancement in the OCG can improve the bridges, hence increasing electrical response to the same content of RH increase.

The OCF-3 h sensor possesses a high sensitivity, following sensing evaluation and demonstration would focus on it. Fig. 3h illustrates the electrical signals of the sensor in absorption-desorption humidity (30%–96% RH) process, where the loading and unloading electrical outputs maintain good consistency, and the response to humidity absorption (Fig. S12) shows remarkable linearity (r^2 =96.87%). We compare the sensor to a commercial humidity detector by placing them in the same humidity environment. There is an outstanding consistency in humidity response (Fig. 3i), and the electrical signals during humidity absorption (Fig. S13) revel a prominent synchronism (r^2 =96.6%). Fig. 3j depicts the sensor is reliable in a series of dynamic and static humidity, where the electrical outputs are highly consistent with the step-by-step increase of RH from 30% to 80%.

3.4. Sensing reliability

Apart from high electrical response, the sensor presents remarkable sensing reliability in complex environments, and negligible dependence to many mechanical inputs. The sensor has high flexibility in shapes (flat, bend, twist, and knot), and more importantly, no matter what shape is, the response to humidity remains a similar level (Fig. 4a). The deformation-resilient property enables the sensor to reliably detect humidity when being wrapped around tubes with various diameters (Fig. 4b). It responds to the humidity in low dependence of bending radius. It ensures humidity sensing reliability considering frequently involved bending in practical wearable and environmental applications. By applying cyclic bending (Fig. 4c) and pressuring (Fig. 4d), the sensor shows insensitivity to the inputs, which is of significance to ensure sensing accuracy by suppressing frequently involved mechanical interference [22,23]. Unlike conventional humidity sensors with weak interaction between sensing materials and substrate [6,7,24], the free-standing sensor displays remarkable wettability and machine-washing ability. Water drops were applied to the sensor and gradually evaporated (Fig. 4e), the cyclically recoverable peaks prove that the sensor is water liquid wettable. Both the resistance (Fig. 4 f) and humidity sensing ability (Fig. 4 g) are stable with minor fluctuation after machine washing for 3 h. As the OCG has high bonding energy with the graphite sheets, which are much higher than the hydrogen bonds, hence the oxidized graphite sheet structure is stable in wetting and washing. Therefore, the moisture sorption and desorption are reversible. It is a significant breakthrough considering humidity-response devices are neither wettable nor washable due to the structure damage of sensors, and/or hydrophilicity and redispersion of active materials to water.

Fig. 4 h shows the temperature in affecting the sensing performance of the sensor. At low temperature (25 °C), the adsorption of water molecules takes a longer time (~400 s) to reach saturated. While at high temperature (>35 °C), it presents a quicker response to the humidity change. Though the response speed difference, the sensor still has a similar electrical change finally. The open porous structure sensor also exhibits high permeability to air (Fig. S14a) and moisture (Fig. S14b) like a piece of cotton cloth, which avoids skin irritation in wearable applications [25]. Based on the above evaluation, the sensor possesses combined merits comparing to state-of-the-art humidity sensors reported (details in Table S2), including tunable initial resistance and sensitivity, high sensing linearity, breathability and flexibility, prominent reliability in withstanding machine washing, various deformations and mechanical inputs.

3.5. Application demonstration in environmental and wearable detection

With the abovementioned sensing superiority, the sensor can be used in broad-range applications from environmental monitoring to noncontact wearable detection. We demonstrate an atmospheric humidity detection system (Fig. 5a) based on the sensor, a drone, and an NFC antenna. Fig. 5b shows the relative resistance change of the sensor when flying from the ground to 50 m height and back, then to 200 m height and back again. The signals are roughly the same in each round with minor fluctuation, which may be attributed to wind-induced humidity undulation. The sensor in 200 m height acquires an intense response, indicating its higher humidity. By measuring the ground RH using a commercial sensor, humidity across the air can be calculated according to the sensor response curves to humidity. Taking advantage of the remarkable wettability, the sensor indicates all-weather detection ability to monitor atmospheric humidity in high humidity and even raining conditions.

Soil water content determination is another critical issue in considering the water content with a dominant impact on soil desertification and plant root growth [26,27]. Two sensors near a plant were assembled inside and above the soil respectively (Fig. 5c). They are used to detect humidity around the plant branches and root soil moisture during watering process. Fig. 5d displays that the soil humidity sharply drops after watering, and gradually recovers with evaporation. By contrast, environment humidity around plant branches slightly decreases after watering, and maintains stable in evaporation process. The RH can also be calculated based on initial humidity level. This demonstration shows the sensor's application prospects in intelligent and customized plant

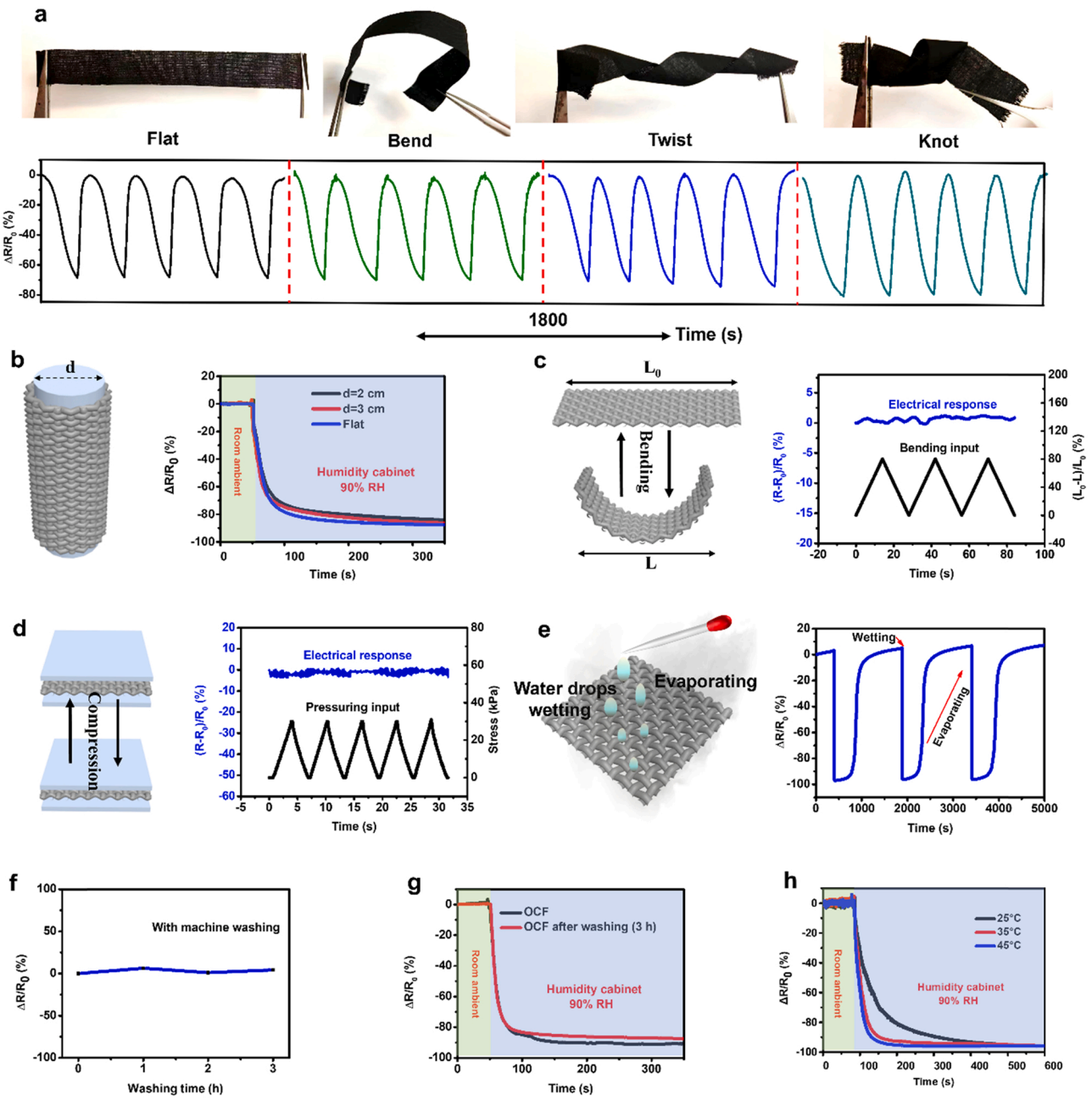

Fig. 4. Humidity sensing reliability of the OCF-3 h sensor. (a) The sensor under different shapes (flat, bend, twist, and knot), and corresponding electrical response in a cyclic RH ranging from 30% to 80%. (b) Schematic diagram of wrapping the sensor around tubes with different diameters, and the electrical outputs while moving in a 90% chamber. (c) Schematic diagram of bending deformation, and corresponding electrical response under cyclic bending (0–80%). The bending is calculated through distance change ($L-L_0$) dividing initial length (L_0). (d) Schematic diagram of pressuring, and corresponding electrical response under cyclic pressuring (0–30 kPa). (e) Illustration of water drops applied on the sensor and gradually evaporated, and corresponding electrical change. (f) Resistance changes of the OCF after machine washing. (g) Humidity sensing comparisons before and after washing. (h) Temperature impact on the sensing performance of the sensor.

cultivating. By putting the sensors in the soil with gradient depth (Fig. S15), electrical outputs during watering can reflect soil drainage, which shows how quickly excess water leaves from the soil. It is an important index in determining soil erosion and land desertification.

Through capturing the water molecules generated from the human body, we demonstrate the sensor in the implementation of wearable noncontact detection. The human mouth contains a large amount of exhaled/inhaled moisture results in a significant electrical resistance response of the OCF sensor (Movie S1). Considering the high breathability, the sensor is very competitive to be embed into a mask with the functions of monitoring cough and speak, as well as recognizing respiration models by integrating with a deep learning network. Fig. S16A displays the electrical change of the sensor generated by coughing, where continuous up-and-down signals are highly consistent with corresponding motion. Also, the slight moisture difference during pronouncing makes it is possible to detect the speaking of various words (Fig. S16b-c). The smart mask equipped with wireless data collect unit (Fig. 5e), and long short-term memory (LSTM) builds up a respiratory recognition system. The LSTM contains two LSTM layers, two dense layers, and a final SoftMax layer (Fig. 5f). The artificial recurrent neural network as an end-to-end architecture can directly take the raw respiratory data as input and classify the data into three classes (i.e., deep, normal, and fast breathing). The respiratory monitoring and discrimination system obtain a high recognition ability with an overall accuracy

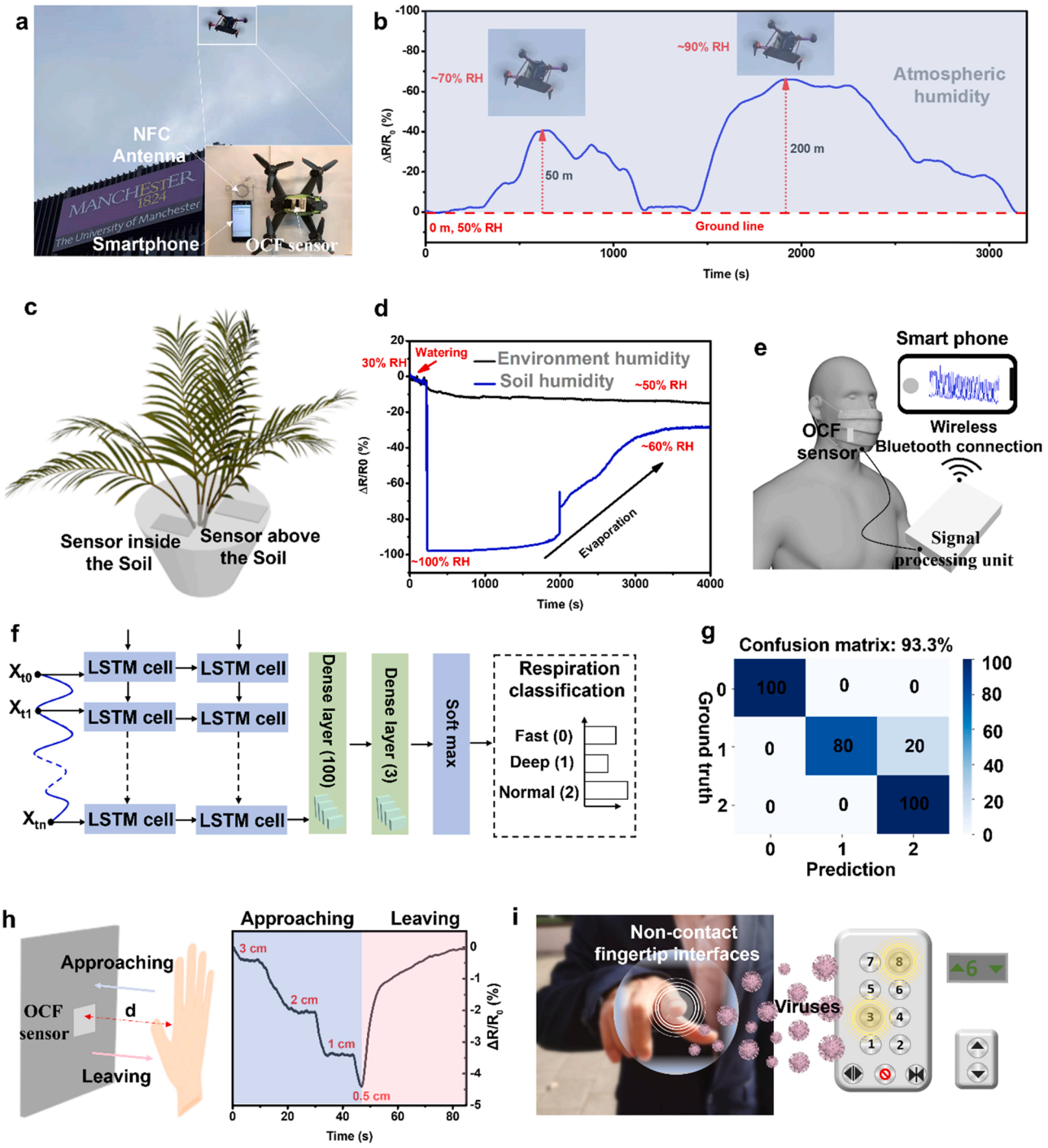

Fig. 5. Application demonstration in environmental and wearable detection. (a) Atmospheric humidity detection system through a platform comprising the sensor, a drone, and an NFC antenna, and (b) corresponding signals. (c) Illustration of the moisture monitoring of a plant by two sensors, and (d) corresponding signals. (e) A smart mask-based on the sensor with wireless data collect unit. (f) An artificial recurrent neural network for respiration identification, and (g) confusion matrix showing the high accuracy in recognizing breathing models. (h) Illustration of hand approaching and leaving and corresponding electrical response of the sensor. (i) Proof-of-concept illustration of non-contact fingertip interfaces.

of 93.3% shown in the confusion matrix in Fig. 5g. The high-precision mask can monitor patients with respiratory diseases, showing feasibility in personal and public digital healthcare.

The interface between a hand and the sensor can be monitored by collecting the electrical signals from the sensor (Fig. 5h). It shows that such response is highly in keeping with corresponding hand approaching and leaving. This also works on the detection of fingertip moving towards the sensor (Fig. S17a), where lower distance leads to a more obvious resistance change (Fig. S17b). The reproducible sensing ability during cyclic forwards and backwards (Fig. S17c), which confirms the sensor can perceive fingertip motions continuously. Taking advantage of the reliable hand/finger non-contact detection, we demonstrate a 3 × 3 sensor array equipped with a multi-channel wireless resistance collection unit for motion reconstruction (Fig. S18). In one scenario, we utilize the array to discriminate the fingertip sliding, showing the fingertip trajectory by writing a slash (Fig. S19a). The electrical signals reveal the distribution is compatible to the position of sliding fingertip across the sensor array from (1, 1) to (3, 3) (Fig. S19b). A more complicated '*T*'

sliding is also precisely reflected by the sensor array (Fig. S19c, d). We also apply the noncontact sensing array in blowing detection. Fig. S20a displays blowing above the center of the sensor array (2, 2). The center shows a higher electrical response, while four corners present a relatively lower electrical change (Fig. S20b). On the other hand, if blowing from one corner (1, 1) (Fig. S20c), the closest point (1, 1) shows the highest response peak, and the rest of the points exhibits a gradient decrease with respect to the distance from the blowing point (Fig. S20d).

By altering the array construction, we demonstrate a gesture monitoring panel, where sensor 1–5 refer to the fingertip from thumb to little finger successively, and sensor 6 represents the palm (Fig. S21a). The resistance change at each point through the stimulation of different hand gestures can accurately monitor corresponding motions in real time (Fig. S21b). These demonstrations successfully show the enormous potential of the sensor in noncontact detection based on fingertips. Fig. 5i presents the potential of the sensor in contactless fingertip interaction interfaces. By integrating the OCF sensor into control panels such as elevator buttons and coded locks, users can remotely perform desired actions through the fingertip, lowering the risk of virus infection. It is a profound revolution to prevent the virus spreading during the covid-19 pandemic.

4. Conclusion

In summary, we have proposed a humidity sensor by controlling the content of humidity-response functional groups on carbonized textiles. It shows outstanding wettability, and machine washability, as well as high reliability upon mechanical stress and geometrical deformations, in contrast to the conventional humidity sensor with poor sensing reliability. It is a significant progress considering humidity sensors are always not washable due to the hydrophilicity and/or redispersion of the active materials to water. The developed sensor exhibits tremendous potential in environment monitoring and governance, wearable digital healthcare with the function of preventing the spread of bacteria and viruses. To the best of our knowledge, this work first reports that carbonized fabric can detect humidity, and the sensitivity is improvable by oxidation. The concept is applicative to cellulose (e.g., linen, hemp, viscose, etc.) and silk (e.g., cocoon and spider silk) materials, as well as many carbonatable polymers. We envision this humidity sensing strategy would arouse attention in flexible humidity sensors using waste textiles, papers, and carbon-based materials (e.g., graphene, carbon nanotube, carbon black) for developing smart green sustainable ecosystem.

CRediT authorship contribution statement

Yangpeiqi Yi: Methodology, Investigation, Data curation. **Chuang Yu**: Data curation. **Heng Zhai**: Investigation. **Lu Jin**: Resources. **Dongxu Cheng**: Methodology. **Yifeng Lu**: Data curation. **Zhongda Chen**: Resources. **Lulu Xu**: Resources. **Jiashen Li**: Resources. **Qinwen Song**: Resources. **Pengfei Yue**: Resources. **Zekun Liu**: Conceptualization, Investigation, Data curation, Writing – original draft, Supervision. **Yi Li**: Supervision, Funding acquisition.

Declaration of Competing Interest

The authors declare that they have no known competing financial interests or personal relationships that could have appeared to influence the work reported in this paper.

Data availability

Data will be made available on request.

Acknowledgments

This work is financially supported by the EU Horizon 2020 through project ETEXWELD-H2020-MSCA-RISE-2014 (Grant No. 644268), the University of Manchester through UMRI project "Graphene-Smart Textiles E-Healthcare Network" (AA14512).

Appendix A. Supporting information

Supplementary data associated with this article can be found in the online version at doi:10.1016/j.nanoen.2022.107780.

References

[1] F. Wang, B. Wang, X. Zhang, M. Lu, Y. Zhang, C. Sun, W. Peng, High sensitivity humidity detection based on functional GO/MWCNTs hybrid nano-materials coated titled fiber Bragg grating, Nanomaterials 11 (2021) 1134.
[2] J.A. Gilbert, B. Stephens, Microbiology of the built environment, Nat. Rev. Microbiol. 16 (2018) 661–670.
[3] S. Van Delden, M. SharathKumar, M. Butturini, L. Graamans, E. Heuvelink, M. Kacira, E. Kaiser, R. Klamer, L. Klerkx, G. Kootstra, Current status and future challenges in implementing and upscaling vertical farming systems, Nat. Food 2 (2021) 944–956.
[4] M. Bariya, H.Y.Y. Nyein, A. Javey, Wearable sweat sensors, Nat. Electron. 1 (2018) 160–171.
[5] M. Bariya, L. Li, R. Ghattamaneni, C.H. Ahn, H.Y.Y. Nyein, L.-C. Tai, A. Javey, Glove-based sensors for multimodal monitoring of natural sweat, Sci. Adv. 6 (2020) eabb8308.
[6] L. Lu, C. Jiang, G. Hu, J. Liu, B. Yang, Flexible Noncontact Sensing for Human–Machine Interaction, Adv. Mater. 33 (2021) 2100218.
[7] L. Xu, H. Zhai, X. Chen, Y. Liu, M. Wang, Z. Liu, M. Umar, C. Ji, Z. Chen, L. Jin, Coolmax/graphene-oxide functionalized textile humidity sensor with ultrafast response for human activities monitoring, Chem. Eng. J. 412 (2021), 128639.
[8] J. Wu, Y.-M. Sun, Z. Wu, X. Li, N. Wang, K. Tao, G.P. Wang, Carbon nanocoil-based fast-response and flexible humidity sensor for multifunctional applications, ACS Appl. Mater. Interfaces 11 (2019) 4242–4251.
[9] L. Ma, R. Wu, A. Patil, S. Zhu, Z. Meng, H. Meng, C. Hou, Y. Zhang, Q. Liu, R. Yu, Full-textile wireless flexible humidity sensor for human physiological monitoring, Adv. Funct. Mater. 29 (2019) 1904549.
[10] T. Li, L. Li, H. Sun, Y. Xu, X. Wang, H. Luo, Z. Liu, T. Zhang, Porous ionic membrane based flexible humidity sensor and its multifunctional applications, Adv. Sci. 4 (2017) 1600404.
[11] L. Xu, Z. Liu, X. Chen, R. Sun, Z. Hu, Z. Zheng, T.T. Ye, Y. Li, Deformation-resilient embroidered near field communication antenna and energy harvesters for wearable applications, Adv. Intell. Syst. 1 (2019) 1900056.
[12] T. Delipinar, A. Shafique, M.S. Gohar, M.K. Yapici, Fabrication and Materials Integration of Flexible Humidity Sensors for Emerging Applications, ACS Omega 6 (2021) 8744–8753.
[13] C. Wang, X. Li, E. Gao, M. Jian, K. Xia, Q. Wang, Z. Xu, T. Ren, Y. Zhang, Carbonized silk fabric for ultrastretchable, highly sensitive, and wearable strain sensors, Adv. Mater. 28 (2016) 6640–6648.
[14] Z. Liu, Z. Li, H. Zhai, L. Jin, K. Chen, Y. Yi, Y. Gao, L. Xu, Y. Zheng, S. Yao, A highly sensitive stretchable strain sensor based on multi-functionalized fabric for respiration monitoring and identification, Chem. Eng. J. (2021), 130869.
[15] C. Wang, M. Zhang, K. Xia, X. Gong, H. Wang, Z. Yin, B. Guan, Y. Zhang, Intrinsically stretchable and conductive textile by a scalable process for elastic wearable electronics, ACS Appl. Mater. Interfaces 9 (2017) 13331–13338.
[16] G. Zhang, S. Sun, D. Yang, J.-P. Dodelet, E. Sacher, The surface analytical characterization of carbon fibers functionalized by H2SO4/HNO3 treatment, Carbon 46 (2008) 196–205.
[17] Y.-R. Shin, S.-M. Jung, I.-Y. Jeon, J.-B. Baek, The oxidation mechanism of highly ordered pyrolytic graphite in a nitric acid/sulfuric acid mixture, Carbon 52 (2013) 493–498.
[18] X. Yan, T. Xu, G. Chen, S. Yang, H. Liu, Q. Xue, Preparation and characterization of electrochemically deposited carbon nitride films on silicon substrate, J. Phys. D: Appl. Phys. 37 (2004) 907.
[19] H.-W. Tien, Y.-L. Huang, S.-Y. Yang, J.-Y. Wang, C.-C.M. Ma, The production of graphene nanosheets decorated with silver nanoparticles for use in transparent, conductive films, Carbon 49 (2011) 1550–1560.
[20] H. Jung, H.K. Choi, S. Kim, H.-S. Lee, Y. Kim, J. Yu, The influence of N-doping types for carbon nanotube reinforced epoxy composites: A combined experimental study and molecular dynamics simulation, Compos. Compos., Part A 103 (2017) 17–24.
[21] S.Y. Cho, Y.S. Yun, S. Lee, D. Jang, K.-Y. Park, J.K. Kim, B.H. Kim, K. Kang, D. L. Kaplan, H.-J. Jin, Carbonization of a stable β-sheet-rich silk protein into a pseudographitic pyroprotein, Nat. Commun. 6 (2015) 7145.
[22] Z. Liu, T. Zhu, J. Wang, Z. Zheng, Y. Li, J. Li, Y. Lai, Functionalized Fiber-Based Strain Sensors: Pathway to Next-Generation Wearable, Electron., Nano-Micro Lett. 14 (2022) 1–39.
[23] Z. Liu, Z. Li, Y. Yi, L. Li, H. Zhai, Z. Lu, L. Jin, J.R. Lu, S.Q. Xie, Z. Zheng, Flexible strain sensing percolation networks towards complicated wearable microclimate and multi-direction mechanical inputs, Nano Energy (2022), 107444.

[24] X. Zhao, L.-Y. Wang, C.-Y. Tang, X.-J. Zha, Y. Liu, B.-H. Su, K. Ke, R.-Y. Bao, M.-B. Yang, W. Yang, Smart Ti3C2T x MXene Fabric with Fast Humidity Response and Joule Heating for Healthcare and Medical Therapy Applications, ACS Nano 14 (2020) 8793–8805.
[25] Z. Liu, K. Chen, A. Fernando, Y. Gao, G. Li, L. Jin, H. Zhai, Y. Yi, L. Xu, Y. Zheng, Permeable graphited hemp fabrics-based, wearing-comfortable pressure sensors for monitoring human activities, Chem. Eng. J. (2020), 126191.
[26] R. Drenovsky, D. Vo, K. Graham, K. Scow, Soil water content and organic carbon availability are major determinants of soil microbial community composition, Microb. Ecol. 48 (2004) 424–430.
[27] K. Vanderlinden, H. Vereecken, H. Hardelauf, M. Herbst, G. Martínez, M.H. Cosh, Y.A. Pachepsky, Temporal stability of soil water contents: A review of data and analyses, Vadose Zone J. (11) (2012) vzj2011.0178.

Yangpeiqi Yi is currently a Ph.D. student in Department of Materials, The University of Manchester, United Kingdom. His current research mainly focuses on ink-based processes for breathable and flexible electronics.

Chuang Yu is a Research Associate in the Cognitive Robotics Lab, Computer Science Department, University of Manchester. He received his Ph. D. degree in Autonomous Systems and Robotics Lab, Institut Polytechnique de Paris, in 2021. His research focuses on trustworthy AI and Robotics, cognitive robotics, human-robot interaction, explainable artificial intelligence (XAI), deep learning, and reinforcement learning.

Heng Zhai received his BSc degree in Textile Science and Technology from The University of Manchester in 2017. After that, he was continuous to a straight doctoral study in the same organization. His Ph.D. research mainly focuses on the fabrication of functional graphene and graphene fiber-based composites for wearable electronics and environmental remediation.

Lu Jin received a BEng degree in textile engineering from Tianjin Polytechnic University, Tianjin, China, MS degree in Polymer Science and Engineering from Dankook University, South Korea, and Ph.D. in Textile Science and Technology from The University of Manchester, Manchester, United Kingdom, in 2006, 2009 and 2021, respectively. His research interests include dry electrodes, unimodal strain sensors, airflow transducers and protective clothing.

Dongxu Cheng is a PhD student at the Department of Mechanical, Aerospace and Civil Engineering, the University of Manchester. His research interests include laser-based multiple materials additive manufacturing, laser micro and nano-processing for functional devices such as batteries, solar cells and bio-implant components.

Yifeng Lu is currently a postgraduate research student in School of Architecture, Hunan University, China. Her research focuses on the investigate the influences of spatial layout of rural residential area on outdoor wind environment.

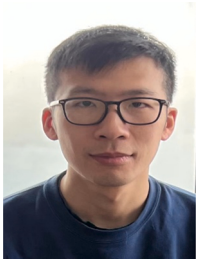

Zhongda Chen recieved his Ph.D. degree at Department of Materials, The University of Manchester, United Kingdom. He is now working as a Postdoc at Nanjing Medical University, PR China. His research area includs fibrious functionalized materials for the development of biomedical devices, implantable electronics and sensors.

Lulu Xu currently works as a research fellow at Wellcome-EPSRC Centre for Interventional and Surgical Sciences (WEISS), University College London (UCL). She received her Ph.D. degree from Manchester University in 2020. Her main research was mainly focused on the development of soft and flexible electronics for wearable applications.

Jiashen Li is a Lecturer in Textile Science & Engineering in Department of Materials, The University of Manchester. He obtained his Ph.D. in polymer materials (physics) from Tianjin University (China) in 2001. He then spent thirteen years conducting biomaterials and fiber spinning in The Hong Kong Polytechnic University, before joining The University of Manchester in 2015. His research interests involve the science and technology underpinning processing-structure-property relationships in functional fibers, textiles and composites.

Qinwen Song recieved her Ph.D. degree at Institute of Textiles and Clothing, The Hong Kong Polytechnic University. She now works in School of Textile Science and Engineering, Xi' an Polytechnic University. Her research interests mainly involve the fabrication, characterization and development of both functional clothes and advanced composites, the test and demonstration of wearable and smart electronics.

Pengfei Yue recieved his MS degree at Institute of Textiles and Clothing, The Hong Kong Polytechnic University. He now works in School of Textile Science and Engineering, Xi' an Polytechnic University. His research interests mainly involve emerging textile materials, innovative textile engineering and technology, wearable and smart electronics based on textile substrates.

Zekun Liu recieved his Ph.D. degree at Department of Materials, The University of Manchester, United Kingdom. He is now working as a Research Associate at Nuffield Department of Orthopaedics, Rheumatology and Musculoskeletal Sciences, University of Oxford. His research interests include nanomaterials and functionalized materials for the development of advanced composites, functional clothes, biomedical devices, and flexible electronics such as sensors, batteries, solar cells, and generators.

Yi Li is a full professor and chair in Textile Science and Engineering in the University of Manchester. He is a Life-Fellow of Royal Society of Art and International Biographical Association and Fellow of the Textile Institute. He is the Chairman of Textile Bioengineering and Informatics Society, deputy council chairman of International Digital Health and Intelligent Materials Innovation Alliance, and board chair of Fashion Big Data Foundation. His research focuses advancement of emerging cross-disciplinary science and engineering of how to design and engineer biomaterials, drug delivery systems, medical devices, smart e-textiles, intelligent wearables for human psychological and physiological needs.